



Ferric (III) complex supported on superparamagnetic $\text{Fe}_3\text{O}_4@SiO_2$ as a reusable Lewis acid catalyst: a new highly efficient protocol for the synthesis of acridinedione and spiroquinazolin-4(3*H*)-one derivatives

Hadi Mohammadi¹ · Hamid Reza Shaterian¹

Received: 9 May 2019 / Accepted: 27 July 2019
© Springer Nature B.V. 2019

Abstract

Nano- $\text{Fe}_3\text{O}_4@SiO_2$ -3,4-dihydroxybenzaldehyde/barbituric acid/phthalhydrazide- FeCl_3 (nano- $\text{Fe}_3\text{O}_4@SiO_2$ -HBP- FeCl_3) was prepared and authenticated by usual analytical and spectroscopic techniques. The prepared nano- $\text{Fe}_3\text{O}_4@SiO_2$ -HBP- FeCl_3 was applied to acridinedione and spiroquinazolin-4(3*H*)-one derivatives under green conditions. In addition, this research offers several advantages such as very easy reaction conditions, simple work-up, excellent yields, high purity of the desired product, short reaction time and one-pot reaction to synthesize $\text{Fe}_3\text{O}_4@SiO_2$ -HBP- FeCl_3 . The recycling studies revealed that catalyst could be easily recovered using an external magnet and reused five times without significant loss of its catalytic activity.

Keywords Nano- $\text{Fe}_3\text{O}_4@SiO_2$ -HBP- FeCl_3 · Superparamagnetic nanocatalyst · Green synthesis · Acridinediones · Spiroquinazolin-4(3*H*)-ones

Introduction

The objective of science is recently shifted toward preserving environment; thus, catalyst recovery and reusability are important properties in catalytic processes [1, 2]. Nanosized metal particles are readily used and intrinsically have a high surface area that provides an excellent accessibility of the surface-bound active catalytic sites [3–9]. One of the important and significant groups of nanoparticles is magnetic

Electronic supplementary material The online version of this article (<https://doi.org/10.1007/s11164-019-03942-w>) contains supplementary material, which is available to authorized users.

✉ Hadi Mohammadi
mohammadi_hadi84@yahoo.com

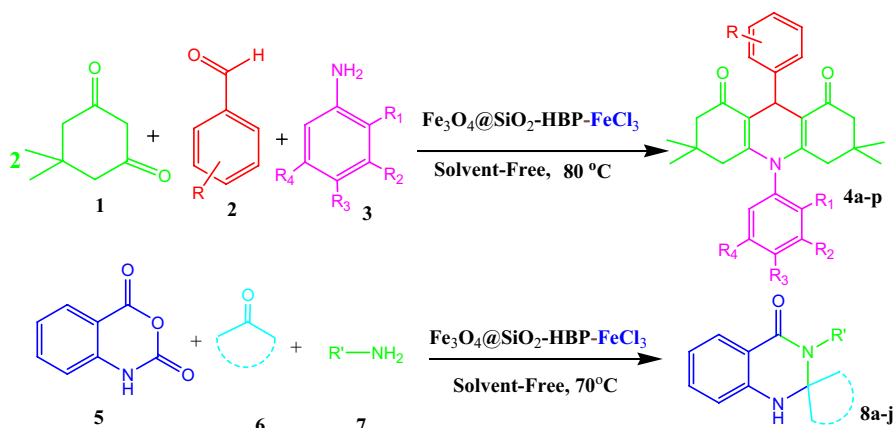
¹ Department of Chemistry, Faculty of Sciences, University of Sistan and Baluchestan, PO Box 98135-674, Zahedan, Iran

nanoparticles (MNPs). Magnetic nanoparticles are of great importance to researchers because of their applications for catalysis [10], and MNPs-based magnetically retrievable catalysis has received considerable attention in synthetic chemistry [11–14]. However, despite substantial progress, research is toward applications of MNPs in the synthesis of magnetically retrievable organocatalysts. MNPs have tendency to form agglomerates to reduce the energy associated with the high surface area-to-volume ratio of the nanosized particles [15], because they are chemically highly active [16]. A solution for this problem is to protect the magnetic core with an outer shell such as silica [17] or polymers [18]. Mostly, silica is used to protect the magnetic core providing appropriate properties, including preventing aggregation, which increases their stability and invariant catalytic activity. Also, the surface silanol groups can be covalently grafted to different organocatalysts [19, 20]. Magnetic core–shell structures of silica such as $\text{Fe}_3\text{O}_4@\text{SiO}_2$ can be easily functionalized by linker groups which can be functionalized by a range of different organocatalysts [21]. In recent years, magnetic nanoparticles (MNPs) (e.g., Fe_3O_4) have been extensively investigated as inorganic catalyst supports the synthesis of organic–inorganic hybrid catalysts [22–24], because of their good stability, easy synthesis, functionalization and high surface area, as well as low toxicity and price [25–27]. Recently, much attention has been focused on the surface modification with appropriate capping agents onto the MNPs surface to anchor the catalytically active complexes. Iron is of considerable interest because of its inexpensive and natural abundance. Iron-based heterogeneous catalyst can promote a variety of organic reactions due to their unique characteristics and properties. Additionally, iron-based heterogeneous catalyst due to high boiling point can be compatible with high-temperature and pressure chemical reactions. Such unique properties of iron further advance the applications of iron as catalyst in many organic transformations [18, 28, 29]. Literature survey showed us that the synthesis of 1,8-dioxo-decahydroacridines is important for researchers because of several activities and applications [30–33]. In the present research, $\text{Fe}_3\text{O}_4@\text{SiO}_2\text{-HBP-FeCl}_3$ as novel nanocatalyst was prepared. All stages from modification and complexation of the surface $\text{Fe}_3\text{O}_4@\text{SiO}_2$ were done in one-pot reaction (Scheme 2). The preparation of 1,8-dioxo-decahydroacridine and spiroquinazolin-4(3*H*)-one derivatives with multi-component condensation reaction of aromatic aldehydes (1.0 mmol), dimedone (2.0 mmol), cyclic ketones (1.2 mmol), isatoic anhydride (1.0 mmol) and primary amines (1.0 mmol) in the presence of nano- $\text{Fe}_3\text{O}_4@\text{SiO}_2\text{-HBP-FeCl}_3$ as nanocatalyst under green conditions was reported for the first time (Scheme 1).

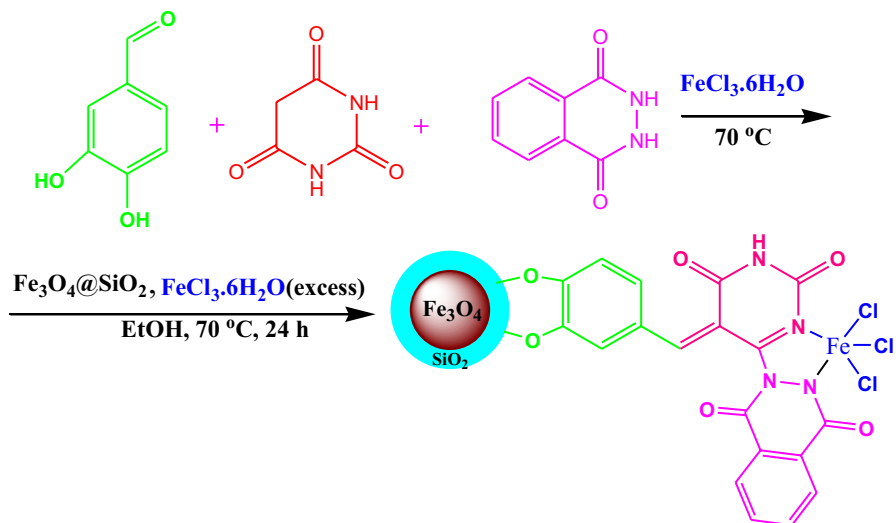
Experimental

Chemicals, instrumentation and analysis

All materials were purchased from Merck and Aldrich companies. ^1H NMR spectra were recorded on a Varian Mercury Plus (300 MHz), a Bruker Avance 300 MHz instruments in $\text{DMSO-}d_6$ as deuterated solvents. Melting points were determined in open capillaries using a BUCHI510 melting point apparatus. Thin-layer



Scheme 1 Synthesis of 1,8-dioxo-decahydroacridine and spiroquinazolin-4(3*H*)-one derivatives in the presence of nano- $\text{Fe}_3\text{O}_4@/\text{SiO}_2\text{-HBP-FeCl}_3$



Scheme 2 Synthesis of $\text{Fe}_3\text{O}_4@/\text{SiO}_2\text{-HBP-FeCl}_3$ nanocatalyst

chromatography (TLC) was performed on silica-gel Poly Gram SIL G/UV 254 plates, and progress of reactions was monitored by TLC. FT-IR spectra were recorded using KBr disks on a JASCO FT-IR 460 plus spectrophotometer. ^1H and ^{13}C -NMR were recorded on an Agilent 300 and 75 MHz spectrometers using TMS as internal standard. Chemical shifts (δ) are reported in ppm. Elemental compositions were determined with a Leo 1450 VP scanning electron microscope equipped with an SC7620 energy-dispersive spectrometer (SEM-EDS) presenting a 133 eV resolution at 20 kV. Power X-ray diffraction (XRD) was performed on a Bruker D8-advance

X-ray diffractometer with Cu K α ($\lambda=0.154$ nm) radiation. The magnetic property was measured by VSM. TGA was done on a thermal analyzer with a heating rate of $10\text{ }^\circ\text{C min}^{-1}$ over a temperature range of $25\text{--}800\text{ }^\circ\text{C}$ under flowing compressed N_2 .

Preparation of $\text{Fe}_3\text{O}_4@\text{SiO}_2\text{-HBP-FeCl}_3$ nanoparticles (Scheme 2)

Fe_3O_4 MNPs were prepared by chemical co-precipitation of Fe^{3+} and Fe^{2+} ions as described in the literature [34]. In a round bottom flask, $\text{FeCl}_3\cdot 6\text{H}_2\text{O}$ (25 mg) was added to a mixture of barbituric acid (1.5 mmol), 3,4-dihydroxybenzaldehyde (1.5 mmol) and phthalhydrazide (1.5 mmol) and the reaction mixture was stirred at $70\text{ }^\circ\text{C}$ in an oil bath for 3 h, according to the literature [35]. After the completion of reaction and formation of product, in this point, solution of $\text{Fe}_3\text{O}_4@\text{SiO}_2$ (500 mg) dispersed in ethanol (50 mL) was added to this reaction mixture and stirred at $70\text{ }^\circ\text{C}$ for another 12 h, whose product loaded onto the surface of the nanoparticles with hydroxyl groups on the aromatic ring. In the following, $\text{FeCl}_3\cdot 6\text{H}_2\text{O}$ (1.5 mmol) was charged to the reaction vessel and the mixture was continuously stirred for 12 h at $70\text{ }^\circ\text{C}$. Finally, $\text{Fe}_3\text{O}_4@\text{SiO}_2\text{-HBP-FeCl}_3$ nanoparticles were removed from solution reaction by using an external magnet and washed several times with ethanol and dried at $60\text{ }^\circ\text{C}$, that Fe complex grafted onto magnetic nanoparticles confirmed by using EDX. And also, superparamagnetic nano-heterogeneous catalyst was characterized by the several techniques such as XRD, FT-IR, VSM, FE-SEM, EDS and TGA. All results confirmed the structure of the $\text{Fe}_3\text{O}_4@\text{SiO}_2\text{-HBP-FeCl}_3$.

General procedure for the direct synthesis 1,8-dioxo-decahydroacridine derivatives using $\text{Fe}_3\text{O}_4@\text{SiO}_2\text{-HBP-FeCl}_3$ nanoparticles as catalyst

$\text{Fe}_3\text{O}_4@\text{SiO}_2\text{-HBP-FeCl}_3$ NMPs (9 mg) was added to a mixture of dimedone (2.0 mmol), aniline derivatives (1.0 mmol) and aromatic aldehydes (1.0 mmol) under solvent-free conditions. The reaction mixture was stirred at $80\text{ }^\circ\text{C}$ in an oil bath. The reaction was monitored by TLC. After the completion of reaction, ethanol was added to reaction mixture to remove the catalyst by an external magnet and purified by crystallization in EtOH. The pure known products were characterized and their physical data were compared with those of known compounds and new products are presented in supplementary information data.

General procedure for the synthesis of spiroquinazolin-4(3H)-one derivatives

Isatoic anhydride (1.0 mmol), primary amine (1.2 mmol), cyclic ketones (1.2 mmol) and $\text{Fe}_3\text{O}_4@\text{SiO}_2\text{-HBP-FeCl}_3$ nanoparticles (7 mg) were stirred at $70\text{ }^\circ\text{C}$. After the completion of the reaction (monitored by TLC), 5 mL CH_2Cl_2 was added and the catalyst was separated by the use of external magnet. Then, CH_2Cl_2 was evaporated. The crude product was purified only by washing with ethanol.

9-(4-Chloro-phenyl)-10-(3,5-dichloro-phenyl)-3,3,6,6-tetramethyl-3,4,6,7,9,10-hexahydro-2H,5H-acridine-1,8-dione (4r) White solid: yield

95%; m.p. 271–273 °C. FT-IR (KBr, ν , cm^{-1}): 3064, 2962, 2890, 1643, 1570, 1485, 1362, 1221, 1009, 841. ^1H NMR (300 MHz, $\text{DMSO-}d_6$, δ , ppm): 7.28–7.97(m, 7H, 2Ar-H), 4.99 (s, 1H, CH), 1.81–2.31 (m, 8H, 4 CH_2), 0.75 (s, 6H, 2 CH_3), 0.93 (s, 6H, 2 CH_3). ^{13}C NMR (75 MHz, $\text{DMSO-}d_6$, δ , ppm):195.54, 150.29, 145.46, 140.95, 135.45, 130.72, 130.25, 129.64,128.28, 113.29, 50.00, 41.27, 32.54, 29.70, 26.56.

9-(4-Bromo-phenyl)-10-(3,5-dichloro-phenyl)-3,3,6,6-tetramethyl-3,4,6,7,9,10-hexahydro-2H,5H-acridine-1,8-dione (4s) White solid: yield 95%; m.p. 277–279 °C. FT-IR (KBr, ν , cm^{-1}): 3054, 2962, 2889, 1643, 1483, 1361, 1222, 1006, 910, 839. ^1H NMR (400 MHz, $\text{DMSO-}d_6$, δ , ppm): 7.29–7.90 (m, 7H, 2Ar-H), 4.98 (s, 1H, CH), 1.81–2.34 (m, 8H, 4 CH_2), 0.75 (s, 6H, 2 CH_3), 0.92 (s, 6H, 2 CH_3). ^{13}C NMR (75 MHz, $\text{DMSO-}d_6$, δ , ppm):195.54, 150.31, 145.88, 140.94, 135.46, 131.21, 130.68, 130.24,119.26, 113.22, 50.00, 41.26, 32.55, 29.70, 26.57.

Results and discussion

Characterization of catalyst

$\text{Fe}_3\text{O}_4@\text{SiO}_2\text{-HBP-FeCl}_3$ nanoparticles were characterized by infrared (FT-IR) spectroscopy, X-ray diffraction (XRD), EDX, field emission scanning electron microscopy (FE-SEM), thermogravimetric analysis (TGA) and vibrating sample magnetometry (VSM).

In XRD, six diffraction peaks have a good concordance with the cubic structure of maghemite (Fe_3O_4) (JCPDS file No. 04-0755). The positions of all the peaks indicated retention of the crystalline structure during functionalization of the Fe_3O_4 , and the grafting process did not change phase of the Fe_3O_4 nanoparticles. The XRD pattern of $\text{Fe}_3\text{O}_4@\text{SiO}_2\text{-HBP-FeCl}_3$ showed that SiO_2 and HBP- FeCl_3 formed amorphous phase in which their patterns showed only patterns of crystalline Fe_3O_4 nanoparticles (Fig. 1).

We provided FE-SEM image which illustrates the catalyst surface morphology that the morphology of the catalyst observed on the SEM micrographs points to

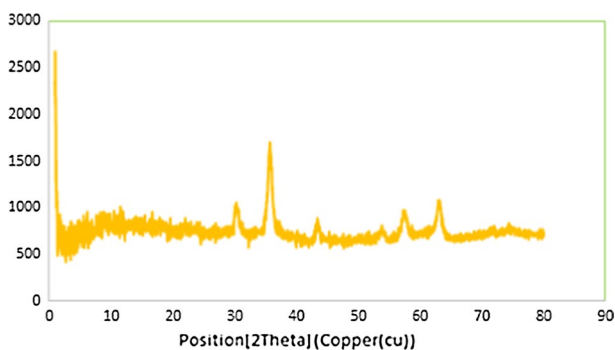


Fig. 1 XRD pattern of $\text{Fe}_3\text{O}_4@\text{SiO}_2\text{-HBP-FeCl}_3$

crystalline phase and an average nanoparticles size of 18 nm using a histogram curve from surface morphology of nano- $\text{Fe}_3\text{O}_4@\text{SiO}_2\text{-HBP-FeCl}_3$ (Fig. 2).

The components of the $\text{Fe}_3\text{O}_4@\text{SiO}_2\text{-HBP-FeCl}_3$ were also analyzed using energy-dispersive X-ray spectroscopy (EDS). The EDS spectrum in Fig. 3 implicates the presence of atoms Fe, O, Si, C, Cl and N in the catalyst which confirms the structure of organometallic compound.

The thermal stability of the $\text{Fe}_3\text{O}_4@\text{SiO}_2\text{-HBP-FeCl}_3$ was investigated by TGA analysis (Fig. 4). Small weight loss occurs below 180 °C, which is due to physically adsorbed solvent and water. A mass loss of 12.5% in the temperature range of 180–520 °C in the TGA curve of $\text{Fe}_3\text{O}_4@\text{SiO}_2\text{-HBP-FeCl}_3$ is mainly

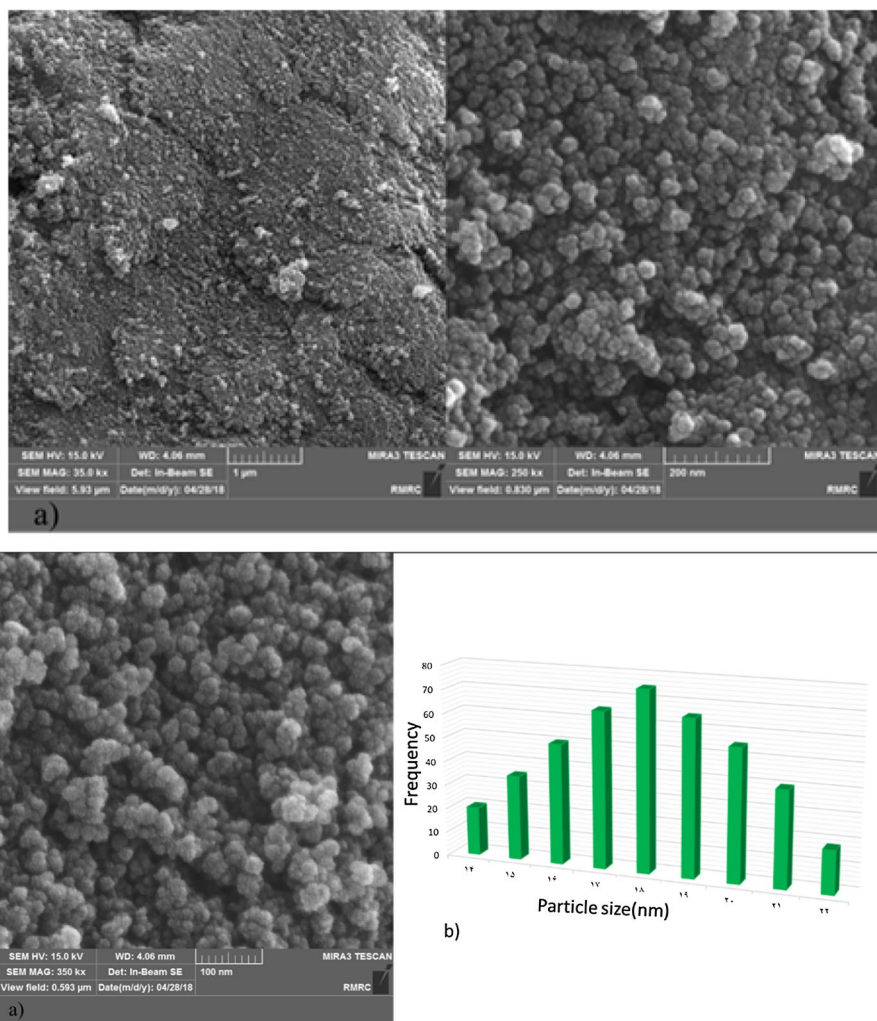


Fig. 2 SEM images of $\text{Fe}_3\text{O}_4@\text{SiO}_2\text{-HBP-FeCl}_3$ (a) and particle size distribution histogram of nanocatalyst (b)

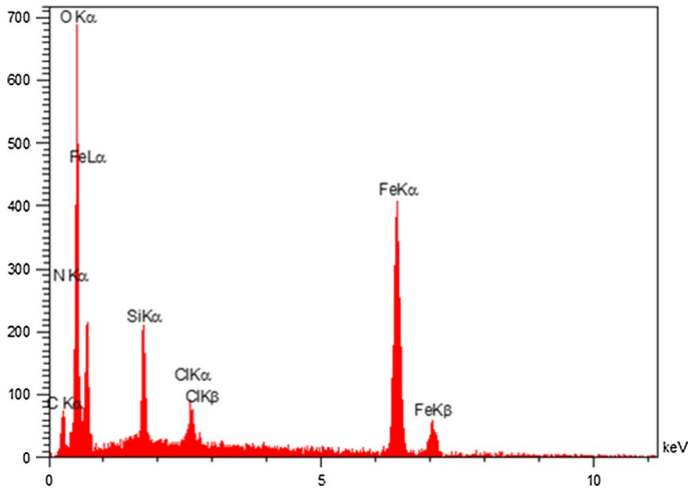
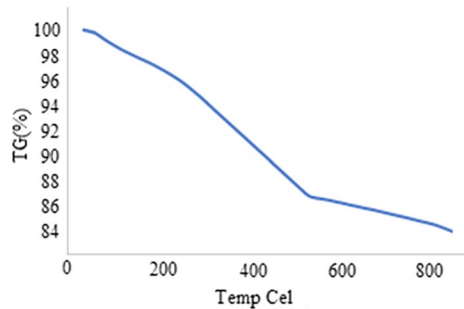


Fig. 3 EDS spectrum of $\text{Fe}_3\text{O}_4@\text{SiO}_2\text{-HBP-FeCl}_3$

Fig. 4 Thermogravimetric analysis of $\text{Fe}_3\text{O}_4@\text{SiO}_2\text{-HBP-FeCl}_3$



attributed to the decomposition of organic groups and FeCl_3 grafted to the $\text{Fe}_3\text{O}_4@\text{SiO}_2$ surface.

The VSM diagram shows the magnetic properties of synthesized catalyst (Fig. 5). The hysteresis loop of $\text{Fe}_3\text{O}_4@\text{SiO}_2\text{-HBP-FeCl}_3$ is measured. Superparamagnetic behavior of the $\text{Fe}_3\text{O}_4@\text{SiO}_2\text{-HBP-FeCl}_3$ illustrates small nanoparticles size of the catalyst. As it can be observed, saturation magnetization value of $\text{Fe}_3\text{O}_4@\text{SiO}_2\text{-HBP-FeCl}_3$ is 47 amu g^{-1} .

The characterization of $\text{Fe}_3\text{O}_4@\text{SiO}_2\text{-HBP-FeCl}_3$ as nanocatalyst was also confirmed by FT-IR spectrum. The peak at $3000\text{--}3400 \text{ cm}^{-1}$ was probably attributed to the NH groups, which is overlapped by the O-H stretching vibration. C-H stretching vibrations appear at 2990 cm^{-1} . The Fe-O stretching vibration was observed at $550\text{--}650 \text{ cm}^{-1}$, and stretching mode of Si-O-Si showed a strong broad peak at about $1099\text{--}1220 \text{ cm}^{-1}$ (Fig. 6).

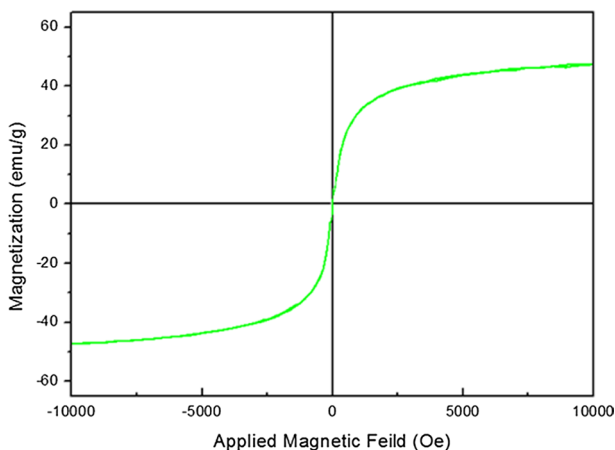


Fig. 5 VSM diagrams of Fe₃O₄@SiO₂-HBP-FeCl₃

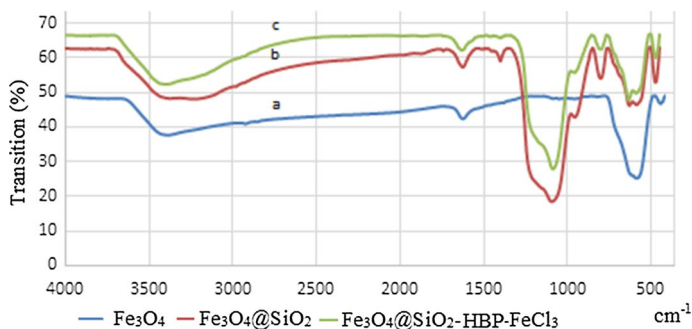
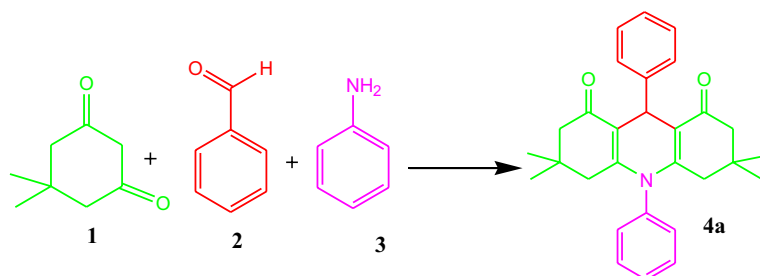


Fig. 6 FT-IR spectra: (a) Fe₃O₄, (b) Fe₃O₄@SiO₂, (c) Fe₃O₄@SiO₂-HBP-FeCl₃

Reaction optimization

After the characterization of the nanocatalyst, in order to establish the optimal conditions for synthesizing of 1,8-dioxo-decahydroacridines in the presence of Fe₃O₄@SiO₂-HBP-FeCl₃ as nanocatalyst, initially, the reaction of dimedone (2.0 mmol), benzaldehyde (1.0 mmol) and aniline (1.0 mmol) was selected as a model reaction. This model reaction with various solvents, temperatures and catalyst amounts was studied to find the best condition. As shown in Table 1, the nature of the solvent was observed to have a profound effect on both the activity of the catalyst and the yield of product.

To select the appropriate conditions for the reaction in the presence of Fe₃O₄@SiO₂-HBP-FeCl₃ as nanocatalyst, first, we chose water/ethanol (1:1) mixture as solvent for this reaction in the presence of Fe₃O₄@SiO₂ and Fe₃O₄@SiO₂-HBP-FeCl₃ as nanocatalyst and catalyst-free condition for model reaction (Table 1, entries 1, 2, 4). So, without catalyst, the time is long and the yield is low. Thus, the reaction does not proceed completely. The yield of desired product was increased when

Table 1 Optimization of reaction conditions for the preparation of 3,3,6,6-tetramethyl-9,10-diphenyl-3,4,6,7,9,10-hexahydroacridine-1,8 (2*H*, 5*H*)-dione

Entry	Catalyst (mg)	Solvent	Temp. (°C)	Time (min)	Yield (%) ^{a,b}
1	Catalyst-free	Solvent-free	80	5h	15
2	Fe ₃ O ₄ @SiO ₂ (10 mg)	H ₂ O/EtOH (1:1) (3 mL)	80	75	60
3	Fe ₃ O ₄ @SiO ₂ -HBP-FeCl ₃ (9 mg)	Solvent-free	50	60	65
4	Fe ₃ O ₄ @SiO ₂ -HBP-FeCl ₃ (9 mg)	H ₂ O/EtOH (1:1) (3 mL)	80	30	75
5	Fe ₃ O ₄ @SiO ₂ -HBP-FeCl ₃ (9 mg)	EtOH (3 mL)	80	30	70
6	Fe ₃ O ₄ @SiO ₂ -HBP-FeCl ₃ (9 mg)	CH ₃ CN (3 mL)	80	50	35
7	Fe ₃ O ₄ @SiO ₂ -HBP-FeCl ₃ (9 mg)	CH ₂ Cl ₂ (3 mL)	40	50	20
8	Fe ₃ O ₄ @SiO ₂ -HBP-FeCl ₃ (9 mg)	H ₂ O (3 mL)	80	30	60
9	Fe ₃ O ₄ @SiO ₂ -HBP-FeCl ₃ (9 mg)	H ₂ O/EtOH (2:1) (3 mL)	80	30	65
10	Fe ₃ O ₄ @SiO ₂ -HBP-FeCl ₃ (9 mg)	H ₂ O/EtOH (1:2) (3 mL)	80	30	85
11	Fe ₃ O ₄ @SiO ₂ -HBP-FeCl ₃ (9 mg)	H ₂ O/EtOH (1:3) (3 mL)	80	30	80
12	Fe ₃ O ₄ @SiO ₂ -HBP-FeCl ₃ (9 mg)	Solvent-free	80	30	95
13	Fe ₃ O ₄ @SiO ₂ -HBP-FeCl ₃ (9 mg)	Solvent-free	70	30	75
14	Fe ₃ O ₄ @SiO ₂ -HBP-FeCl ₃ (9 mg)	Solvent-free	90	30	95
15	Fe ₃ O ₄ @SiO ₂ -HBP-FeCl ₃ (5 mg)	Solvent-free	80	30	75
16	Fe ₃ O ₄ @SiO ₂ -HBP-FeCl ₃ (7 mg)	Solvent-free	80	30	85
17	Fe ₃ O ₄ @SiO ₂ -HBP-FeCl ₃ (11 mg)	Solvent-free	80	30	95
18	Fe ₃ O ₄ @SiO ₂ -HBP (10 mg)	Solvent-free	80	50	78

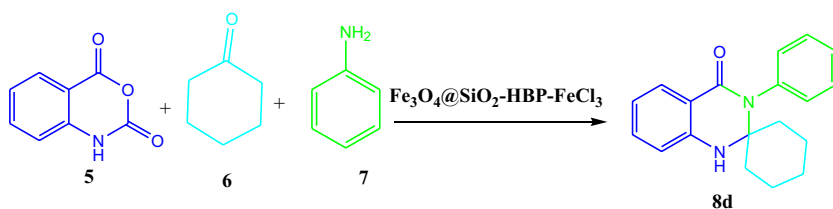
^aReaction conditions: the reaction of dimedone (2.0 mmol), benzaldehyde (1.0 mmol) and aniline (1.0 mmol)

^bYields refer to isolated pure product

the reaction was done in the presence of Fe₃O₄@SiO₂-HBP-FeCl₃ as nanocatalyst (Table 1, entry 3). This reaction was tested in water as green solvent and organic solvents such as ethanol, dichloromethane, acetonitrile and water/ethanol mixture and also in solvent-free condition. The best performance of Fe₃O₄@SiO₂-HBP-FeCl₃ was achieved at 80 °C under solvent-free condition (Table 1, entry 12). To illustrate the effect of FeCl₃ in nanocatalyst on yield of reaction, model reaction in the presences of Fe₃O₄@SiO₂-HBP shows 75% in comparison with 95% in the presence of Fe₃O₄@SiO₂-HBP-FeCl₃ (Table 1, entries 12, 18). In order to assess the effect of

temperature on the reaction, we carried out the reactions at various temperatures as shown in (Table 1, entries 3, 12, 13, 14). Catalytic activity increases with increasing temperature at 80 °C. Use of a higher temperature had no significant effect on the reaction rate or the isolated yield of product (Table 1, entry 14). The effect of the catalyst amount of the reaction was also investigated (Table 1, entries 12, 15, 16, 17). Use of a higher amount of catalyst had no significant effect on the reaction rate or the isolated yield of product, while a decrease in the amount of catalyst decreased the product yield. The best result was obtained using 9 mg of catalyst. Overall, the ideal reaction conditions for the formation of 1,8-dioxo-decahydroacridine derivatives were under solvent-free condition and 9 mg of the catalyst at 80 °C (Table 1, entry 12).

Table 2 Preparation of spiroquinazolin-4(3*H*)-one in the presence of Fe₃O₄@SiO₂-HBP-FeCl₃



Entry	Catalyst	Reaction conditions	Time (min)	Yield (%) ^{a,b}
1	Fe ₃ O ₄ @SiO ₂ -HBP-FeCl ₃ (7 mg)	H ₂ O (3 mL) (80 °C)	60	65
2	Fe ₃ O ₄ @SiO ₂ -HBP-FeCl ₃ (7 mg)	EtOH (3 mL) (80 °C)	60	70
3	Fe ₃ O ₄ @SiO ₂ -HBP-FeCl ₃ (7 mg)	H ₂ O/EtOH (1:1) (3 mL) (80 °C)	60	75
4	Fe ₃ O ₄ @SiO ₂ (8 mg)	Solvent-free (70 °C)	60	65
5	Fe ₃ O ₄ @SiO ₂ -HBP-FeCl ₃ (7 mg)	CH ₃ CN (3 mL) (80 °C)	60	55
6	Fe ₃ O ₄ @SiO ₂ -HBP-FeCl ₃ (7 mg)	CH ₂ Cl ₂ (3 mL) (35 °C)	90	35
7	Catalyst-Free	Solvent-free (90 °C)	120	No
8	Fe ₃ O ₄ @SiO ₂ -HBP-FeCl ₃ (7 mg)	Solvent-free (70 °C)	50	92
9	Fe ₃ O ₄ @SiO ₂ -HBP-FeCl ₃ (7 mg)	Solvent-free (25 °C)	75	40
10	Fe ₃ O ₄ @SiO ₂ -HBP-FeCl ₃ (7 mg)	EtOH (3 mL) (25 °C)	75	25
11	Fe ₃ O ₄ @SiO ₂ -HBP-FeCl ₃ (7 mg)	Solvent-free (50 °C)	65	70
12	Fe ₃ O ₄ @SiO ₂ -HBP-FeCl ₃ (7 mg)	Solvent-free (60 °C)	60	80
13	Fe ₃ O ₄ @SiO ₂ -HBP-FeCl ₃ (7 mg)	Solvent-free (80 °C)	50	92
14	Fe ₃ O ₄ @SiO ₂ -HBP-FeCl ₃ (5 mg)	Solvent-free (70 °C)	50	70
15	Fe ₃ O ₄ @SiO ₂ -HBP-FeCl ₃ (6 mg)	Solvent-free (70 °C)	50	87
16	Fe ₃ O ₄ @SiO ₂ -HBP-FeCl ₃ (8 mg)	Solvent-free (70 °C)	50	92
17	Fe ₃ O ₄ @SiO ₂ -HBP (7 mg)	Solvent-free (70 °C)	50	75

^aReaction conditions: isatoic anhydride 1 (1.0 mmol), aniline 2 (1.2 mmol) and cyclohexanone 4 (1.2 mmol) in different conditions

^bYield refers to isolated pure products

Optimization of different parameters in synthesis of spiroquinazolin-4(3H)-one derivatives

At the onset of this research, we investigated the model one-pot three-component cyclocondensation reaction using stirring between isatoic anhydride (1 mmol), aniline (1.2 mmol) and cyclohexanone (1.2 mmol) to optimize the reaction parameters.

We investigated the reaction without using any solvent in the absence of catalyst, and no reaction occurred (Table 2, entry 7). After that, we investigated the reaction in the presence of $\text{Fe}_3\text{O}_4@\text{SiO}_2\text{-HBP-FeCl}_3$ under solvent-free condition at 25 °C (Table 2, entry 9). Then, we studied the model reaction in the presences of $\text{Fe}_3\text{O}_4@\text{SiO}_2\text{-HBP-FeCl}_3$ catalyst in the EtOH solvent at 25 °C. The yield was lower for ethanol (Table 2, entry 10); different solvents were studied such as H_2O , EtOH, $\text{H}_2\text{O}/\text{EtOH}$, CH_3CN , CH_2Cl_2 and solvent-free condition in the presence of $\text{Fe}_3\text{O}_4@\text{SiO}_2\text{-HBP-FeCl}_3$ catalyst (Table 2, entries 1–8). Among all the solvents and solvent-free condition, $\text{Fe}_3\text{O}_4@\text{SiO}_2\text{-HBP-FeCl}_3$ gives the best result under solvent-free condition at 70 °C (Table 2, entry 8). The effect of temperature was also investigated. The model reaction was conducted in three different temperatures (Table 2, entry 8, 9, 11, 12, 13), as can be seen, the highest yield was attained at 70 °C. The effect of amount of catalyst was studied by using the model reaction. As the amount

Table 3 Synthesis of 1,8-dioxo-decahydroacridines catalyzed by $\text{Fe}_3\text{O}_4@\text{SiO}_2\text{-HBP-FeCl}_3$ (9 mg) nanoparticles at 80 °C under solvent-free condition

Entry	R	R ₁ , R ₂ , R ₃ , R ₄	Product	Time (min)	Yield (%) ^{a,b}	Observed M.p (°C)	Lit. M.p (°C) [References]
1	H	H, H, H, H	4a	30	95	203–205	252–254 [36]
2	4-OMe	H, H, H, H	4b	35	94	201–203	216–218 [36]
3	4-Me	H, H, H, H	4c	35	93	205–207	259–261 [36]
4	4-Br	H, H, H, H	4d	25	95	206–208	253–255 [36]
5	3- Br	H, H, H, H	4e	30	92	244–246	250–252 [36]
6	H	H, H, Me, H	4f	25	90	159–161	259–261 [36]
7	H	H, Me, H, H	4g	35	91	194–196	262–264 [37]
8	H	H, H, Cl, H	4h	25	90	219–221	301–303 [36]
9	3-NO ₂	H, H, Cl, H	4i	30	93	214–216	285–287 [37]
10	4-OCH ₃	H, H, Cl, H	4j	35	92	247–249	255–257 [37]
11	4-Me	H, H, Cl, H	4k	35	93	216–218	262–265 [37]
12	4-Br	H, H, Cl, H	4l	25	95	263–265	304–300 [37]
13	H	H, H, Br, H	4m	25	95	301–303	303–305 [37]
14	4-NO ₂	OH, H, H, H	4n	40	92	296–298	296–298 [37]
15	4-Me	H, H, Me, H	4o	35	94	295–297	296–298 [38]
16	OH	H, H, Me, H	4p	40	90	> 300	352–354 [38]
17	4-Cl	H, Cl, H, Cl	4q	30	95	271–273	New compound
18	4-Br	H, Cl, H, Cl	4r	30	95	277–279	New compound

^aReaction conditions: the reaction of dimedone (2.0 mmol), aromatic aldehydes (1.0 mmol) and aniline derivatives (1.0 mmol)

^bYields refer to isolated pure product

Table 4 Synthesis of spiroquinazolin-4-(3*H*)-one derivatives in the presence of Fe₃O₄@SiO₂-HBP-FeCl₃ as nanomagnetic catalyst

Entry	Cycloketone	R'	Products	Time (min)	Yield (%) ^{a,b}	Observed M.p (°C)	Lit. M.p (°C), [Ref]
1	Cyclopentanone	Phenyl	8a	50	90	203–205	204–206 [39]
2	Cyclopentanone	4-Me-phenyl	8b	50	91	208–209	208 [39]
3	Cyclopentanone	4-OMe-phenyl	8c	55	89	206–208	207–210 [39]
4	Cyclohexanone	Phenyl	8d	50	92	215	215 [39]
5	Cyclohexanone	4-Me-phenyl	8e	50	93	210–212	209–211 [39]
6	Cyclohexanone	4-OMe-phenyl	8f	60	91	223–225	224–226 [39]
7	Cyclohexanone	Phenethylamine	8g	50	94	151–153	150–152 [40]
8	Cycloheptanone	Phenethylamine	8h	65	85	146–148	146–147 [40]
9	Tetrahydro-pyran-4-one	Phenethylamine	8i	60	85	181–183	181–183 [40]
10	Tetrahydro-thiopyran-4-one	Phenethylamine	8j	65	87	172–174	171–173 [40]

^aReaction conditions: isatoic anhydride (1.0 mmol), amines (1.2 mmol) and cyclic ketones (1.2 mmol)^bYield refers to isolated pure products

Table 5 Comparison of the efficiency of various catalysts with the $\text{Fe}_3\text{O}_4@\text{SiO}_2\text{-HBP-FeCl}_3$ in the synthesis of 1,8-dioxo-decahydroacridines^(a) and spiroquinazolin-4(3*H*)-one^(b)

Entry	Catalyst	Conditions	Time (min)	Yield (%)	References
1	Pt NPs@rGO	EtOH/H ₂ O, 90 °C	60	94	[37] ^(a)
2	(PVP-SO ₃ H) HSO ₄	EtOH/H ₂ O, reflux	30	95	[38] ^(a)
3	Proline	EtOH: H ₂ O, reflux	360	79	[41] ^(a)
4	Amberlyst-15	CH ₃ CN, reflux	300	81	[42] ^(a)
5	[Hmim]TFA	Solvent-free, 80 °C	270	86	[43] ^(a)
6	Silica-bonded S-sulfuric acid	EtOH, reflux	120	94	[44] ^(a)
7	cobalt–alanine metal complex	EtOH, Reflux	60	96	[45] ^(a)
8	$\text{Fe}_3\text{O}_4@\text{SiO}_2\text{-HBP-FeCl}_3$	Solvent-free, 80 °C	30	95	This work ^(a)
9	$\text{Fe}_3\text{O}_4@\text{SiO}_2@\text{TiO}_2\text{-OSO}_3\text{H}$	DES, 60 °C	60	90	[39] ^(b)
10	$\text{Fe}_3\text{O}_4@\text{SiO}_2\text{-HBP-FeCl}_3$	Solvent-free, 70 °C	50	92	This work ^(b)

of catalyst increased, the time of the reaction decreased and the yield of reaction increased. As can be seen, the highest yield (92%) belonged to the use of 7 mg of catalyst.

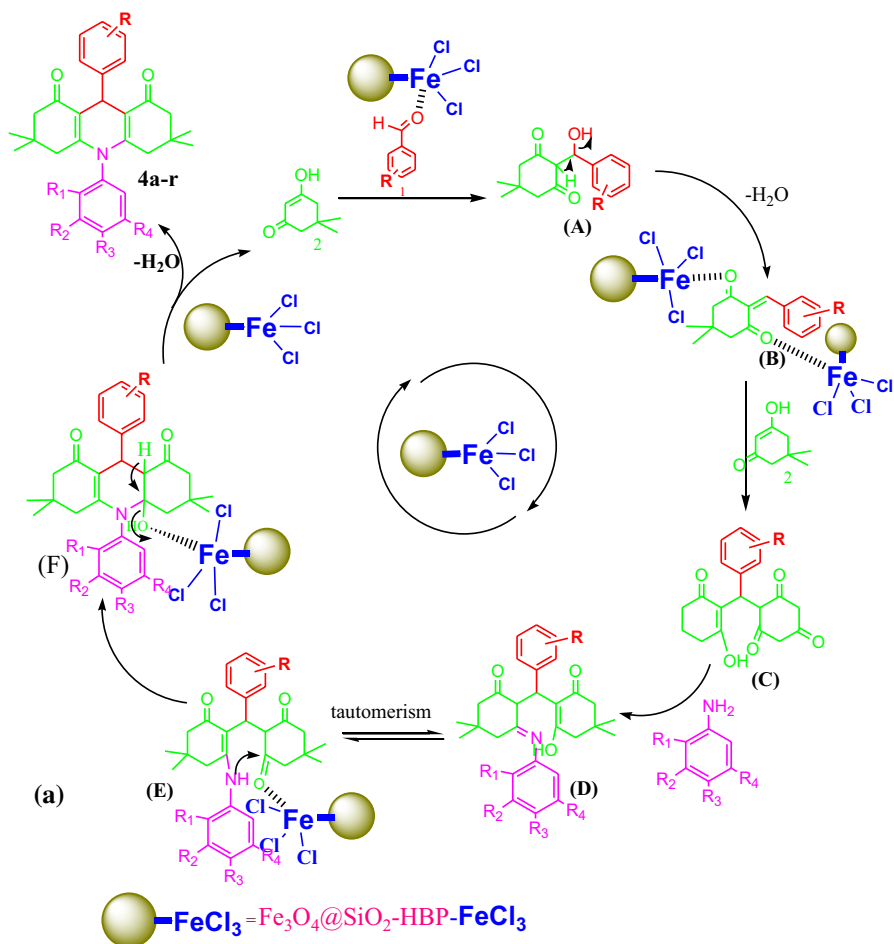
According to optimal considered conditions, some 1,8-dioxo-decahydroacridines and spiroquinazolin-4(3*H*)-ones were synthesized and results are shown in Tables 3, 4. The obtained results indicate that the reactions can proceed well enough with a relatively wide range of aromatic substituted benzaldehydes or cyclic ketones and anilines containing electron-donating and electron-withdrawing groups.

The results shown in Table 5 demonstrated that our present method is more efficient than that of the reported methods. Additionally, the present catalyst seems to be more beneficial from a green chemistry and commercial point of view.

Mechanism

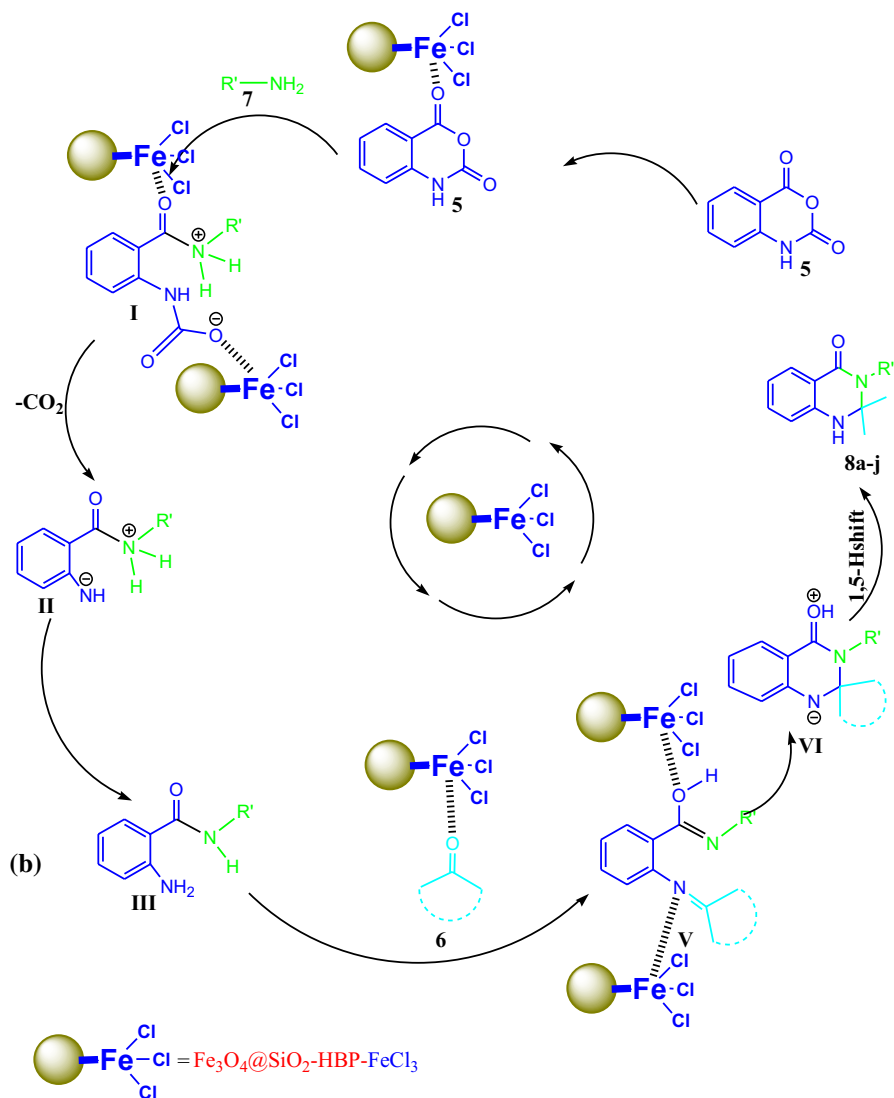
According to the literature [36], the proposed mechanism is for the synthesis of 1,8-dioxo-decahydroacridine derivatives in the presence of $\text{Fe}_3\text{O}_4@\text{SiO}_2\text{-HBP-FeCl}_3$ nanocatalyst (Scheme 3a). First, the intermediate (**A**) was formed via condensation reaction of aromatic aldehydes (1) with dimedone (2) in the presence of $\text{Fe}_3\text{O}_4@\text{SiO}_2\text{-HBP-FeCl}_3$ nanocatalyst and then intermediate (**A**) with the removal of group water converted to intermediate (**B**) and then, with Michael addition another molecule dimedone to intermediate (**B**) to form intermediate (**C**). Then, the intermediate (**D**) was obtained from the reaction of aniline derivatives (3) with intermediate (**C**). Subsequently, intermediate (**D**) with tautomerization converted to intermediate (**E**), in which the intramolecular nucleophilic attack by the enolic NH group (**H**) leads to the formation of the intermediate (**F**); now this intermediate with removal of molecule water was converted to final products (**4a–r**).

The mechanism for the formation of the desired product was suggested according to the literature [39]. First, iron of catalyst is coordinated to the oxygen atom of the carbonyl group on isatoic anhydride to activate them for the nucleophilic



Scheme 3 The proposed mechanism for the synthesis of 1,8-dioxo-decahydroacridine and spiroquinazolin-4(3H)-one derivatives catalyzed by $\text{Fe}_3\text{O}_4 @ \text{SiO}_2\text{-HBP-FeCl}_3$ as Lewis acid nanocatalyst

attack of the amines to produce an intermediate **I** which in turn affords intermediate **II** through decarboxylation. The proton transfer of intermediate **II** affords 2-amino-*N*-substituted-amide **III**. The tautomerization of amide group in intermediate **III** could be catalyzed in the presence of the supported metal. Subsequently, the reaction of activated aldehydes or cyclic ketones with 2-amino-*N*-substituted-amide **III** proceeds to afford the imine intermediates **IV**, **V**. The imine moiety in intermediate **IV**, **V** is also activated by catalyst. Cyclization of **IV**, **V** to intermediate **VI**, **VII** occurs via intramolecular nucleophilic attack of nitrogen on imine carbon. Then, 1,5-proton shift gives the final desired products (Scheme 3b).



Scheme 3 (continued)

Recycling and reusing of the catalyst

The reusability of the $\text{Fe}_3\text{O}_4@SiO_2\text{-HBP-FeCl}_3$ was studied via the synthesis of 5,3,3,6,6-tetramethyl-9,10-diphenyl-3,4,6,7,9,10-hexahydroacridine-1,8-dione (4a, reaction model) under optimized conditions. It was concluded that the $\text{Fe}_3\text{O}_4@SiO_2\text{-HBP-FeCl}_3$ nanocatalyst could be reused five times without any significant reduction in product yield (Fig. 7).

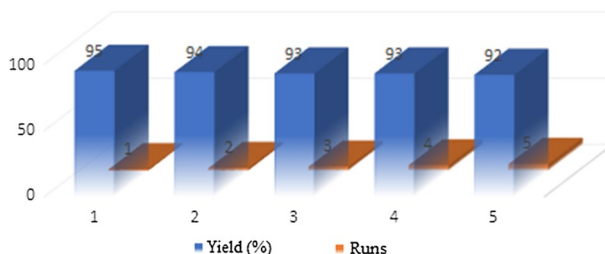


Fig. 7 Reusability of $\text{Fe}_3\text{O}_4@\text{SiO}_2\text{-HBP-FeCl}_3$ as Lewis acid nanocatalyst

Conclusion

We use a simple and effective method for synthesizing organometallic compound supported on nanoparticles surface in which preparation of the ligand, supporting and formation of the complex at the surface of the nanoparticles were carried out in one-pot reaction for the preparation of $\text{Fe}_3\text{O}_4@\text{SiO}_2\text{-HBP-FeCl}_3$ nanocatalyst. And also, we have developed a simple, facile, green and efficient protocol for multi-component synthesis of 1,8-dioxo-decahydroacridine and spiroquinazolin-4(3*H*)-one derivatives by using $\text{Fe}_3\text{O}_4@\text{SiO}_2\text{-HBP-FeCl}_3$ as a novel organometallic heterogeneous nanomagnetic catalyst. The products were obtained with easy reaction conditions, excellent yields within short reaction time, simple work-up and avoidance of toxic organic solvents. The nanocatalyst can be conveniently separated and recovered from the reaction system by magnet and can be reused five times without substantial loss in catalytic activity.

Acknowledgements We gratefully appreciate the University of Sistan and Baluchestan Research Councils for the financial support of this work.

References

1. Z. Nasresfahani, M.Z. Kassaee, E. Eidi, *Appl. Organomet. Chem.* **31**, e3800 (2017)
2. P. Kumar, K. Kadyan, M. Duhan, J. Sindhu, K. Hussain, S. Lal, *Chem. Pap.* **73**, 1153 (2019)
3. R.K. Sharma, M. Yadav, M.B. Gawande, *ACS Symp. Ser.* **1238**, 1 (2016)
4. S. Gandhi, N. Nagalakshmi, I. Baskaran, V. Dhanalakshmi, M.R. Gopinathan, N.R. Anbarasan, *J. Appl. Polym. Sci.* **118**, 1666 (2010)
5. T. Demirci, B. Çelik, Y. Yıldız, S. Eriş, M. Arslan, F. Sen, B. Kilbas, *RSC Adv.* **6**, 76948 (2016)
6. E. Esmā, Y. Yunus, K. Benan, Ş. Fatih, *J. Nanosci. Nanotechnol.* **16**, 5944 (2016)
7. F. Şen, G. Gökağaç, S. Şen, *J. Nanopart. Res.* **15**, 1979 (2013)
8. R. Ayranci, G. Baskaya, M. Guzel, S. Bozkurt, M. Ak, A. Savk, F. Sen, *Nano-Struct. Nano-Objects* **11**, 13 (2017)
9. Y. Yildiz, T.O. Okayay, B. Sen, B. Gezer, S. Kuzu, A. Savk, E. Demir, Z. Dasedelen, H. Sert, F. Sen, *ChemistrySelect* **2**, 697 (2017)
10. Z. Tai, M.A. Isaacs, L.J. Durndell, C.M.A. Parlett, A.F. Lee, K. Wilson, *Mol. Catal.* **449**, 137 (2018)
11. A. Mirhashemi, M.A. Amrollahi, *Res. Chem. Intermed.* **45**, 2549 (2019)
12. M.M. Khodaei, A. Alizadeh, M. Haghipour, *Res. Chem. Intermed.* **45**, 2727 (2019)
13. M. Gholamhosseini-Nazari, S. Esmati, K.D. Safa, A. Khataee, R. Teimuri-Mofrad, *Res. Chem. Intermed.* **45**, 1841 (2019)

14. S.V. Sokolov, E. Kätelhön, R.G. Compton, *J. Phys. Chem. C* **119**, 25093 (2015)
15. M.F. Silva, A.A.W. Hechenleitner, J.M. Irache, A.J.A. de Oliveira, E.A.G. Pineda, *J. Mater. Sci.* **18**, 1400 (2015)
16. V. Polshettiwar, R.S. Varma, *Green Chem.* **12**, 743 (2010)
17. R.N. Baig, R.S. Varma, *Chem. Commun.* **48**, 6220 (2012)
18. M. Sheykhani, A. Yahyazadeh, L. Ramezani, *Mol. Catal.* **435**, 166 (2017)
19. A. Bamoniri, N. Moshtael-Arani, *RSC Adv.* **5**, 16911 (2015)
20. N. Azgomi, M. Mokhtar, *J. Mol. Catal. A Chem.* **398**, 58 (2015)
21. M.A. Bodaghifard, S. Asadbegi, Z. Bahrami, *J. Iran. Chem.* **14**, 365 (2017)
22. M.A. Zolfigol, M. Safaiee, N. Bahrami-Nejad, *New J. Chem.* **40**, 5071 (2016)
23. F. Javaheri, S. Hassanajili, *J. Appl. Polym. Sci.* **133**, 48 (2016)
24. A. Ghorbani-Choghamarani, G. Azadi, *Appl. Organomet. Chem.* **30**, 247 (2016)
25. M.A. Zolfigol, M. Kiafar, M. Yarie, A.A. Taherpour, M. Saeidi-Rad, *RSC Adv.* **6**, 50100 (2016)
26. Q. Dai, Y. Wang, W. Xu, Y. Liu, Y. Zhou, *Mikrochim. Acta* **184**, 4433 (2017)
27. S.A. Hamrahian, J. Rakhshshah, S.M. Mousavi Davijani, S. Salehzadeh, *Appl. Organomet. Chem.* **10**, e4501 (2018)
28. H.A. Patel, A.M. Sawant, V.J. Rao, A.L. Patel, A.V. Bedekar, *Catal. Lett.* **147**, 2306 (2017)
29. D. Sahu, A.R. Silva, P. Das, *RSC Adv.* **5**, 78553 (2015)
30. H. Singh, J.K. Rajput, G. Govil, P. Arora, J. Badhan, *Appl. Organomet. Chem.* **10**, e4514 (2018)
31. M. Esmaeilpour, A.R. Sardarian, H. Firouzabadi, *Appl. Organomet. Chem.* **32**, e4300 (2018)
32. A. Burak, P. Handan, K. Muharrem, S. Fatih, J. Nanosci. *Nanotechnol.* **16**, 6498 (2016)
33. R. Ulus, Y. Yıldız, S. Eriş, B. Aday, F. Şen, *ChemistrySelect* **1**, 3861 (2016)
34. X. Liu, Z. Ma, J. Xing, H. Liu, *J. Magn. Magn. Mater.* **270**, 1 (2004)
35. V.R. Mudumala, R.R. Chinthaparthi, T. Yeon, *Tetrahedron* **70**, 3762 (2014)
36. Z. Zarei, B. Akhlaghinia, *New J. Chem.* **41**, 15485 (2017)
37. B. Aday, Y. Yıldız, R. Ulus, S. Eris, F. Sen, M. Kaya, *New J. Chem.* **40**, 748 (2016)
38. H.R. Safaei, M. Safaei, M. Shekouhy, *RSC Adv.* **5**, 6797 (2015)
39. A. Maleki, T. Kari, M. Aghaei, *J. Porous Mater.* **24**, 1481 (2017)
40. X. Zhu, S.-R. Kang, L. Xia, J. Lee, N. Basavegowda, Y.-R. Lee, *Mol. Divers.* **19**, 67 (2015)
41. K. Venkatesan, S.S. Pujari, K.V. Srinivasan, *Synth. Commun.* **39**, 228 (2009)
42. B. Das, P. Thirupathi, I. Mahender, V. Saidi Reddy, Y.K. Rao, *J. Mol. Catal. A Chem.* **247**, 233 (2006)
43. M. Dabiri, M. Baghbazadeh, E. Arzroomchilar, *Catal. Commun.* **9**, 939 (2008)
44. K. Niknam, F. Panahi, D. Saberi, M. Mohagheghnejad, *J. Heterocycl. Chem.* **47**, 292 (2010)
45. M.M. Alam, A.T. Mubarak, M.A. Assiri, S.M. Ahmed, *BMC Chem.* **13**, 40 (2019)

Publisher's Note Springer Nature remains neutral with regard to jurisdictional claims in published maps and institutional affiliations.